Effect of TEMPO-oxidization and rapid cooling on thermo-structural properties of nanocellulose

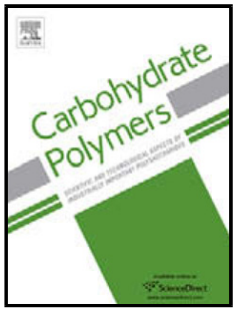

Title: Effect of TEMPO-Oxidization and Rapid Cooling on Thermo-Structural Properties of Nanocellulose

Authors: Mhd Abd Cader Mhd Haniffa, Yern Chee Ching, Cheng Hock Chuah, Yong Ching Kuan, Nik Nazri, Luqman Chuah Abdullah, Liou Nai-Shang

PII: S0144-8617(17)30609-4
DOI: http://dx.doi.org/doi:10.1016/j.carbpol.2017.05.084
Reference: CARP 12370

To appear in:

Received date: 26-12-2016
Revised date: 1-5-2017
Accepted date: 25-5-2017

Please cite this article as: Mhd Haniffa, Mhd Abd Cader., Ching, Yern Chee., Chuah, Cheng Hock., Kuan, Yong Ching., Nazri, Nik., Abdullah, Luqman Chuah., & Nai-Shang, Liou., Effect of TEMPO-Oxidization and Rapid Cooling on Thermo-Structural Properties of Nanocellulose.*Carbohydrate Polymers* http://dx.doi.org/10.1016/j.carbpol.2017.05.084

Effect of TEMPO-Oxidization and Rapid Cooling on Thermo-Structural Properties of Nanocellulose

Mhd Abd Cader Mhd Haniffa[1,2], Yern Chee Ching[1,*], Cheng Hock Chuah[2], Yong Ching Kuan[3], Nik Nazri[4], Luqman Chuah Abdullah[5], Liou Nai-Shang[6]

[1]Department of Chemical Engineering, Faculty of Engineering, University of Malaya, 50603 Kuala Lumpur, Malaysia
[2]Department of Chemistry, Faculty of Science, University of Malaya, 50603 Kuala Lumpur, Malaysia
[3] University of Reading Malaysia, Persiaran Graduan, Kota Ilmu, Educity, 79200 Iskandar Puteri, Johor, Malaysia
[4]Department of Mechanical Engineering, Faculty of Engineering, University of Malaya, 50603 Kuala Lumpur, Malaysia
[5] Institutes of Tropical Forestry and Forest Product (INTROP), University Putra Malaysia, Serdang 43400, Malaysia
[6] Department of Mechanical Engineering, Southern Taiwan University of Science and Technology, Tainan City 710, Taiwan R.O.C.

Highlight :

- Cellulose nanofibrils (CNFs) were prepared from MCC using TEMPO-oxidation.
- Acid hydrolyzed nanocrystalline celluloses (NCCs) was treated with TEMPO-oxidation.
- Thermo-structural properties and thermogravimetric analysis of the nanocellulose were investigated with respect to rapid cooling treatment.
- Rapid cooling treatment improve thermo-structural properties of the nanocelluloses
- TEMPO-oxidation and rapid cooling treatment contributes to the fabrication of NCCs with a high number of carboxyl entities and admirable thermal stability.

Abstract

Recently, surface functionality and thermal property of the green nanomaterials have received wide attention in numerous applications. In this study, microcrystalline cellulose (MCC) was used to prepare the nanocrystalline celluloses (NCCs) using acid hydrolysis method. The NCCs was treated with TEMPO [(2,2,6,6-tetramethylpiperidin-1-yl)oxy radical]-oxidation to prepare TEMPO-oxidized NCCs. Cellulose nanofibrils (CNFs) also prepared from MCC using TEMPO-oxidation. The effects of rapid cooling and chemical treatments on the thermo-structural property studies of the prepared nanocelluloses were investigated through FTIR,

thermogravimetric analysis-derivative thermogravimetric (TGA-DTG), and XRD. *A posteriori* knowledge of the FTIR and TGA-DTG analysis revealed that the rapid cooling treatment enhanced the hydrogen bond energy and thermal stability of the TEMPO-oxidized NCC compared to other nanocelluloses. XRD analysis exhibits the effect of rapid cooling on pseudo 2_1 helical conformation. This was the first investigation performed on the effect of rapid cooling on structural properties of the nanocellulose.

Keywords: Nanocellulose; TEMPO-oxidation; Rapid cooling; Thermal stability; Hydrogen bond energy; TGA-DTG

1. Introduction

Cellulose is a biopolymer used in numerous industrial applications. This biopolymer has several applications (Abitbol et al., 2016; Choo, Ching, Chuah, Sabariah, Liou, 2016; Nandgaonkar, Krause, & Lucia, 2016) as a novel physical and chemical reinforcement in nanocomposite materials (Cao, Dong, & Li, 2007; De France, Chan, Cranston, & Hoare, 2016; Thennakoon, Ching, & Chuah, 2017) because of its high mechanical strength (El Miri et al., 2016; Li, Cao, Cao, Guo, & Lu, 2016; Siqueira, Bras, & Dufresne, 2008), shear assembly and di-electrophoresis behaviour (Csoka, Hoeger, Peralta, Peszlen, & Rojas, 2011). Cellulose is a linear syndiotactic homopolymer composed of d-anhydroglucopyranose units which are linked by β-(1→4)-glycosidic bonds (Qiu and Hu, 2013).

Nanocelluloses typically include nanowhiskers or nanocrystalline celluloses (NCC) obtained from the mechanical disintegration of an acid hydrolyzed (e.g. 63.5 wt% sulfuric acid) cellulose/water slurry of native celluloses; TEMPO-oxidized cellulose nanofibrils (NFS); and nanofibrillated celluloses obtained from recurrent twin-screw extruder or high-pressure homogenizer treatments for chemically modified or unmodified cellulose/water slurries (Pääkkö et al., 2007, Aulin et al., 2009; Okita, Fujisawa, Saito, & Isogai, 2010; Thennakoon, Ching, Kuan, Chuah, Luqman, 2017).

The nanoscale structure and chemically modified surface-treated cellulose significantly modify the colloidal stability, optical, and thermo- and dynamic-mechanical properties of nanocomposite films (Helbert, Cavaille, & Dufresne, 1996; Henriksson & Berglund, 2007; Siqueira et al., 2008; Zhong, Fu, Peng, Zhan, & Sun, 2012; Jonoobi et al., 2015; Sampath, Ching, Chuah, Sabariah, Lin, 2016). Furthermore, physico-chemical treatments, oxidation approaches (Montanari, Roumani, Heux, & Vignon, 2005; Soni & Mahmoud, 2015), and reaction conditions including temperature, pH,

concentration, equimolar ratio, and oxidizing period (Carlsson, Lindh, Nyholm, Strømme, & Mihranyan, 2014; Soni & Mahmoud, 2015), affect the electro-structural properties, such as ζ-potential (Zhong et al., 2012), dielectric and magnetic properties (De France, Yager, Hoare, & Cranston, 2016; Munier, Gordeyeva, Bergström, & Fall, 2016), crystallinity (Carlsson et al., 2014), and carboxylation (Fujisawa, Okita, Fukuzumi, Saito, & Isogai, 2011) of TEMPO-oxidized nanocelluloses.

TEMPO-oxidation technique is the most commonly used chemical pre-treatment method for modifying the surface of the native cellulose selectively under aqueous and mild conditions (Missoum, Belgacem, & Bras, 2013; T Saito, Okita, Nge, Sugiyama, & Isogai, 2006). TEMPO is a mild oxidant with auxiliary co-oxidants, including NaClO or NaBrO, which can regenerate the oxidizing system; the TEMPO/NaBr/NaClO and TEMPO/NaClO/$NaClO_2$ systems have been extensively used for surface-limited cellulose carboxylation at pH 9–10 and ~5, respectively (Carlsson et al., 2014). These systems respectively generate approximately 1.7 and 0.8 mmol g^{-1} sodium carboxylate group during the oxidation of microcrystalline cellulose with respect to the pH level (Fujisawa et al., 2011). Interestingly, TEMPO-oxidation do not affect the structural properties of the nanocelluloses (Habibi, Chanzy, & Vignon, 2006). The advantage of this technique is it can selectively converting the C6 primary hydroxyl groups of the polysaccharides into charged carboxyl entities via the C6 aldehyde groups without oxidizing the secondary hydroxyls (De Nooy, Besemer, & van Bekkum, 1995; Goh, Ching, Chuah, Luqman, Liou, 2016). TEMPO-oxidation pre-treatment is usually followed by a mechanical treatment wherein, the energy consumption of the mechanical disintegration can be drastically decreased to value less than 7 MJ/kg as compared to nanofibrils fabrication using repeated cycles of a high pressure homogenizer (700–1400 MJ/kg) (Missoum et al., 2013). Due to the repulsive forces among the ionized carboxylic acids, this enable the nanofibrils within the fibres to separate better from each other (Eichhorn et al., 2010). In addition, the supernatant of the pre-treated cellulose/water slurry by TEMPO-oxidation is usually considered as smaller and thinner carboxylic functionalized cellulose nanofibrils compared to enzymatic pre-treated nanofibrils (Missoum et al., 2013).

In addition to the mechanical isolation treatment (J. Li et al., 2012), chemical functionalization, and electro isolation methods, (Isogai, Saito, & Isogai, 2011; Kalita et al., 2015; Khalil et al., 2014; Morán, Alvarez, Cyras, & Vázquez, 2008; Novo, Bras, García, Belgacem, & Curvelo, 2015; Salajková, Berglund, & Zhou, 2012; Soni & Mahmoud, 2015), rapid cooling is a sophisticated and tranquil technique which can be used to alter the thermo-structural properties of the nanomaterials. The

rapid cooling technique employs flexible and faster temperature alterations in the reaction system which could significantly affect the surface, thermal properties, macromolecular structural stability, and ordered structure of the crystals growth behavior of the nanomaterials. The colloidal (Zhong et al., 2012), viscous (Shafeiei-Sabet, Hamad, & Hatzikiriakos, 2013), viscoelastic (Lu, Hemraz, Khalili, & Boluk, 2014), rheological (Ching et al., 2016; Shafeiei-Sabet et al., 2013), and dynamic rheological phase behaviors (Chen et al., 2013) of nanocrystalline celluloses has been studied and (Mhd Haniffa, Ching, Abdullah, Poh, & Chuah, 2016) incorporated with several reaction conditions. Nonetheless, the effects of rapid cooling on the pseudoplastic, morphological, electrical, and crystalline structure of nanocelluloses have not been clarified. Moreover, the effect of rapid cooling on thermo-structural properties of nanocellulose is uncommon in literature.

Here, three types of nanocellulose particles: TEMPO-oxidized CNFs, acid-hydrolyzed NCC, and TEMPO-oxidized NCC were prepared in this study to observe the thermo-structural properties of the as-prepared nanocelluloses under rapid cooling treatment. The mechanism by which rapid cooling treatment alters the thermo-structural properties and crystalline nature of the nanocelluloses were explored. The effects of rapid cooling and multiple chemical treatments on the degree of crystallization were quantified using wide angle X-ray scattering. The crystallization degree of the rapidly cooled nanocellulose was compared with those of non-cooled nanocellulose and MCC. Moreover, we investigated the responses of dynamic stability of intermolecular and intra-molecular hydrogen bonds between the polymeric chains of nanocelluloses against rapid cooling as well as its effects on the pseudo 2_I helical conformation of the nano-crystals within the crystalline structure of the nanocellulose. To the best of our knowledge, this study is the first to analyse the effect of rapid cooling on nanocelluloses on the basis of the thermo-structural properties and crystalline nature of the nanocelluloses.

Experimental Methodology

2.1. Materials

Commercial microcrystalline cellulose (MCC) powder (wood source, DP 650) was purchased from Sigma-Aldrich, whose carboxyl content was 0.05 mmol/g with the average crystal size of 20 μm and has out of 90% of the α-cellulose content. Sulfuric acid (97%) for hydrolysis, sodium bromide, 6–14% sodium hypochlorite solution, TEMPO [(2,2,6,6-tetramethylpiperidin-1-yl)oxy radical], sodium hydroxide, and other chemicals (analytical grade) were purchased from Sigma-

Aldrich and used without any purification. Purified water from Millipore Milli-Q purification system was used for all the analysis.

2.2. Preparation of rapid cooled TEMPO-oxidized CNFs

The CNFs were prepared according to a known procedure (De Nooy et al., 1995) with some modifications. In-deeply, the oxidation process started with 1wt% MCC using TEMPO/NaBr/NaClO system with the mole ratio of 0.1 mmol / 0.9 mmol / 8 mmol/g cellulose in 100 ml Millipore water. The pH of the system was reduced and controlled to pH 10 using drops of 0.1 M HCl and 0.5 M NaOH respectively. The reaction mixture was allowed to oxidize for 300-360 min then quenched by 10 mL of ethanol followed by 10 fold of cold Millipore water with temperature of 4 °C. The sodium ion was exchanged by adjusting the pH 2–3 using 0.1 M HCl and allowed to settle for 120 min. The CNFs were separated by vacuum filtration and the suspension was then mechanically disintegrated using ultrasonic homogenizer (Dyna-Ken WT500: Benchtop/Manual) with 10 mm diameter probe tip at 60 Hz and 500 W output power followed by ultra-sonication for 10 min. Ultra-sonicated CNFs were stored at 4 °C for one week. The supernatant was decanted and centrifuged for 20 min at 5071 RCF. The resultant slurry was then freeze-dried to get the TEMPO-treated CNF and labelled as TRC-4. The same method was used to prepare TRC-12, except that 10-fold Millipore water with temperature of 12 °C was used instead of 4 °C.

2.3 Preparation of uncooled TEMPO-oxidized CNFs

Uncooled TEMPO-oxidized CNFs were prepared following the same method in TRC preparation, except that 10-fold Millipore water with room temperature was used instead of cold Millipore water. The prepared uncooled CNF sample was labelled as TUC. The yields of the samples were listed in Table 1.

2.4 Preparation of rapidly cooled acid hydrolysed NCCs

MCC hydrolysis was performed with some modifications as described previously (Hamad & Hu, 2010). In brief, 10.2 g of MCC was isolated using 64% sulfuric acid hydrolysis at 45 °C for 130 min with a stoichiometric ratio of 3.4 mL sulfuric acid/g celluloses. Hydrolysis was controlled and then quenched by adding 10 fold of cold Millipore water with temperature of 4°C. The resultant slurry was allowed to settle overnight at 4°C. The supernatant was then decanted, and the remaining pure white suspension was centrifuged at 5071 RCF for 20 min. After removal of

supernatant, the remaining suspension was centrifuged for 20 min with Millipore water to complete five centrifugation cycles.

Finally, the resultant suspension was placed into dialysis membrane tube with a 14,000 molecular weight cut-off and allowed to dialyze against pure running water for one week. The neutral NCC suspension was ultra-sonicated for 20 min at room temperature and freeze-dried to obtain NCC. The sample was labelled as ARC-4 and this method was followed to prepare ARC-12, except that 10-fold of Millipore water with temperature of 12 °C was used instead of 4 °C.

2.5 Preparation of uncooled acid hydrolysed NCCs

Uncooled acid hydrolysed NCCs were prepared following the same method used in ARC preparation, except that 10-fold Millipore water with room temperature was used instead of cold Millipore water. The sample was labelled as AUC and the yields of the samples were listed in Table 1.

2.6. TEMPO oxidation treatment on cooled and uncooled acid hydrolysed NCCs

TEMPO-oxidation treatment also performed on ARC and AUC samples to modify the hydroxymethyl groups of the NCC synthesized from acid hydrolyses method as described above. The prepared samples were labelled as TARC-4, TARC-12 and TAUC separately. The yields of the samples were included in Table 1.

2.7. Characterization of study

2.7.1. Fourier transform infrared (FTIR)

The functional groups on the surface of the nanocelluloses were confirmed via FTIR spectroscopy and compared with those on the surface of MCC. Moreover, these spectra were used to determine the structural characteristics of the nanocelluloses on the basis of the peak areas and height. The nanocelluloses powders were dispersed into the KBr matrix at 1:100 ratios. Compressed transparent KBr pellets were utilized to analyze the spectra in transmittance mode with 32 scans, at a resolution of 4 cm^{-1} and a wavenumber range of 400 to 4000 cm^{-1}.

The following equations were used to examine the effect of rapid cooling on hydrogen bond energy and hydrogen bond distance of the OH stretching mode of the nanocelluloses (Poletto, Ornaghi, & Zattera, 2014).

$$E_H = \frac{1}{k}\left(1 - \frac{\breve{\upsilon}}{\breve{\upsilon}_0}\right) \quad (1)$$

$$R = \frac{1}{b}(\breve{v} - \breve{v}_0 + c) \qquad (2)$$

where E_H and R is the hydrogen bonds energy and distance respectively; $\breve{v}_0$ is the standard stretching frequency of the free OH groups at 3650 cm^{-1}; $\breve{v}$ is the frequency of the bonded OH groups; k = 3.81 × 10^{-6} kJ; and b, c are constant i.e $b = 4430, c = 12.581 \times 10^3$.

2.7.2. Thermogravimetric analysis (TGA)

The thermal stability of the nanocelluloses was studied via TGA and then compared with that of MCC. Nanocellulose with a net weight of 10 mg was utilized for thermogravimetric analysis (TGA) and derivative thermogravimetry (DTG) using a TGA 8516 (Mettler-Toledo DmbH thermoanalyzer), where the samples were heated to 800 °C under nitrogen atmosphere at room temperature with a heating rate of 20 °C /min.

2.7.3. X-ray diffractograms (XRD)

XRD of the nontreated and the TEMPO-treated nanocelluloses were examined using Siemens D5000 system. The samples were X-rayed using monochromatic Ni-filtered Cu Kα radiation with a wavelength of 1.542 Å. The generator was operated at 40 kV and 40 mA, and the diffracted intensity data were measured between the ranges of 5° ≤ 2θ ≥ 50°, using 0.05° scan steps with a counting rate of 1.5°/min. The following empirical formula (Hermans & Weidinger, 1948) was used to calculate the crystalline index (*CrI*) of the nontreated and the TEMPO-treated nanocelluloses and compared with MCC.

$$CrI(\%) = \frac{A_{crystal}}{A_{crystal} + A_{amorphous}} \times 100 \qquad (3)$$

where, $A_{crystal}$ is the sum of lattice diffraction peaks areas and $A_{amorphous}$, is given by the total amorphous area of X-ray diffraction pattern.

3 Results and discussion

3.1. Effect of rapid cooling on structural property of the nanocelluloses

The FTIR spectra of the nanocelluloses are illustrated in Fig. 1. The fluctuating broad band at 3440 and 1035 cm^{-1} correspond to the free O–H stretching modes of the OH groups and C–O ether groups in nanocellulose respectively (Poletto et al., 2014, Thennakoon, Ching, Chuah, Ramesh, Lin, 2017). Sharp asymmetric and weak symmetric C–H peaks were observed at 2902 and 2845 cm^{-1} respectively in all spectra (Mok, Ching, Muhamad, Abu Osman, Ramesh, 2017). These peaks can be

attributed to methyl and methylene groups respectively. Results showed that these peaks were exposed to insignificant level of extractive contents, such as methyl- and methylene-containing organic extratives (Tang, Yang, Zhang, & Zhang, 2014). TEMPO-oxidized nanocelluloses exhibited a new peak at 1730 cm^{-1}, attributed to the C=O stretching vibration of the dimer carboxyl or the aldehyde absorption that might originated from the TEMPO-oxidation of the hydroxymethyle groups in nanocelluloses (Poletto et al. 2014). The FTIR spectra failed to assign the C=O stretching vibration of monomeric carboxyl group at 1760 cm^{-1}. However, the obverted intra-molecular hydrogen bond (dimeric carboxyl groups) at 1730 cm^{-1} was shifted towards lower frequency region of 1718 cm^{-1} after rapid cooling. Consequently, TEMPO-oxidized CNFs and NCC might have strong intra-molecular hydrogen bonds within the polymeric chain network. (Ching, Rahman, Ching, Sukiman, Cheng, 2015; Martinez-Felipe et al., 2016; Salas, Nypelö, Rodriguez-Abreu, Carrillo, & Rojas, 2014).

The FTIR spectra are influenced by the presence of water. In fact a previous computational analysis (Baird, Hamlin, O'Sullivan, & Whiting, 2008; Lee et al., 2015) has reported that a strong cellulose-water interaction was found theoretically on cellulose molecules. The formation of shape peak at 1640 cm^{-1} was attributed to the bending of the –OH group (Liao et al., 2016). The obtained peak was observed in all spectra of the NCCs and MCC, even after same careful drying process. Moreover, the stretching frequency of this –OH group was overlapped with the –OH stretching frequency of the NCCs at 3440-3346 cm^{-1}. However, this study focuses on the effect of rapid cooling on in-plane and out-plane deformation such as twisting, wagging or stretching vibration of the different groups in NCCs such as C–O, C–H, -O–H at 1111, 1035 and 937 cm^{-1} (Yokoi et al., 2003) respectively. The collective FTIR areas of these peaks were used for analysis and denoted as EOH.

Furthermore, the observed bending vibration of the equatorial –OH group at 937 cm^{-1} was significantly changed after cooling treatment. This phenomenon might be attributed to either the macromolecular disorder of the NCCs or the intra–molecular attractions (Koosha, Mirzadeh, Shokrgozar, & Farokhi, 2015). The out-plane deformation was not observed in any of the spectrum of nanocelluloses, indicating that all chemical and mechanical treatments were deformed in the external surface, excluding the hydroxymethyle (C6–OH) (Poletto et al. 2014; Yokoi et al. 2003). The finite order of the crystallites of the nanocelluloses is dependent on the ring torsion effect (Neyertz et al., 2000), wherein the peak area between 695–715 cm^{-1} was used to evaluate this effect with respect to the rapid cooling treatment as shown in Fig. 2.

3.2. *Effect of rapid cooling on hydrogen bond energy of nanocelluloses*

The hydrogen bond energy and bond distance of the OH stretching of nanocelluloses calculated using Equations (1) and (2) respectively are listed in Table 1. In the present study, the OH starching frequency within 3436–3346 cm^{-1} was observed and used to evaluate the effect of rapid cooling on hydrogen bond energy of the nanocelluloses (J. Li et al., 2012; Poletto et al., 2014). The respective frequencies of TRC-4, and TARC-4 at 3413, and 3425 cm^{-1} could be comparable with that of TUC, and TAUC at 3436 and 3439 cm^{-1} indicating the effects of rapid cooling on hydrogen bond energy. The hydrogen bond distance (R) of the intra-molecular, inter-chain, and inter-sheet interactions of the hydroxyl groups are considered to study the effect of rapid cooling on their starching vibration (Eyley & Thielemans, 2014). Both of the TRC-4 and TARC-4 has shown lower R value and higher E_H values compared to TUR and TAUC respectively. This result has indicated that the rapid cooling has significant impact on the hydrogen bond distance of the nanocelluloses (Poletto et al., 2014).

However, TEMPO-oxidized nanocelluloses demonstrated lower E_H and higher R-values than the acid hydrolyzed NCC. Moreover, the MCC exhibited the lowest E_H value but a higher R-value compared to nanocelluloses (Poletto et al., 2014). By contrast, the R and E_H values of the acid hydrolyzed NCC demonstrated that the thermal energy from rapid cooling was only used for neutralization. Consequently, E_H value of ARC-4 dramatically decreased with increasing R-value compared with that of AUC.

3.3 *A posteriori study of chemical and rapid cooling treatments of nanocelluloses*

A posteriori study of the FTIR spectra was clearly elaborated by the peak parameter such as peak height, peak area etc for the analysis of nanocelluloses. The band in the FTIR spectra at 895 cm^{-1} is attributed to the amorphous system, whereas the band at 1430 cm^{-1} is assigned to the crystalline nature (Fig. 1) (Åkerholm, Hinterstoisser, & Salmén, 2004). The ratio between these peak heights was used to analyze the lateral order index (LOI) of the nanocelluloses. Total crystallinity index (TCI) was analyzed based on the peak height ratio of the corresponding bands at 1372 and 2900 cm^{-1} (Fig. 1) (Carrillo, Colom, Sunol, & Saurina, 2004; Corgié, Smith, & Walker, 2011; Poletto et al., 2014).

The hydrogen bonding intensity (HBI) was examined based on the peak height ratio of the corresponding bands at 3440 and 1318 cm^{-1} (Fig. 1) (Poletto et al., 2014). Equatorial -OH fluctuation, stretching C–O, and ring asymmetric stretching against the chemical and rapid cooling treatments

were evaluated using the peak areas of the bands at 937, 1035-1055, and 1111 cm^{-1} (Carrillo et al., 2004) respectively; hereafter, the total area of these peaks is denoted as EOH. However, the significant differences in a posteriori study of the LOI, TCI, HBI and EOH were not observed among rapid cooled nanocelluloses.

The degree of crystallization is proportional to the TCI (Carrillo et al., 2004; Corgié et al., 2011). Consequently, the TCI, HBI, and EOH values are higher in TARC-4 than in TAUC. The HBI and EOH values were lower in the ARC-4 spectra than in the AUC spectra but TCI was higher in the former because of rapid cooling (Fig. 2(a)). The EOH was doubled for TARC-4 than TAUC because of the enhancements in the frequencies of the ring asymmetric stretching, and C–O stretching as well as in the number of bound water molecules (Lee et al., 2015). Consequently, the peak area results proved the effects of rapid cooling on the structural properties of the samples (Fan, Dai, & Huang, 2012). The rapidly cooled nanocelluloses had better crystalline structures than those uncooled and were comparable with MCC (Fig. 2(b)). However, the crystalline orientation was entirely changed, which was clarified by the peak area results of the finite order (García, Ruiz-Blanco, Marrero-Ponce, & Sotomayor-Torres, 2016) (Fig. 2(b)).

3.4 *Effect of rapid cooling on crystalline structure of the nanocelluloses*

The crystalline characteristic peaks of the nanocelluloses were observed in diffractograms at 2θ = 14.8°, 16.5°, 22. 5° and 34.6° and their crystallographic planes d($1\bar{1}0$), d(110), d(200) and d(004) were labeled in Fig. 3 as recommended previously (Novo et al., 2015; Wada, Heux, & Sugiyama, 2004; Rubentheren, Ward, Chee, Nair, 2015), wherein the effect of chemical and rapid cooling treatments on the intensities of the peaks were analyzed. ARC-4, TAUC and TARC-4 exhibited a high peak at 14.8° of the crystallographic plane d($1\bar{1}0$) with an increasing trend than the peak at 16.5° of the crystallographic plane d(110). The same trend was observed in MCC and AUC as shown in Fig. 3(a). The 2θ reflection of cellulose II was assigned to the crystallographic planes of d($1\bar{1}0$)and d(110) at 12.4°, and 20.0° respectively (Novo et al., 2015). Moreover, cellulose II exhibits the lowest minimum energy with local minima in orientation compared to other six structures of the cellulose, namely $I_\alpha, I_\beta, III_I, III_{II}$ IV_I, IV_{II} allomorphs (Eyley & Thielemans, 2014).

The TARC-4 and AUC diffractograms exhibited the existence of cellulose II in the crystallographic planes of d($1\bar{1}0$) and d(110) at 12.4°, and 20.0° respectively (Fig. 3(b) & 3(c)). The rapid cooling and the hydrolyzation energy had dominated to form cellulose II in TARC-4 and AUC respectively. In this study, the acid hydrolysis has caused the formation of low-DP cellulose, which is partly soluble in acidic water at cold condition. Moreover, these once-dissolved low-DP celluloses are precipitated on crystalline cellulose I particles for forming cellulose II as a sort of regenerated cellulose. However, TEMPO-oxidation did not affect the structural properties of the nanocelluloses (Habibi et al., 2006).

The effects of rapid cooling treatment on pseudo 2_I helical conformation of the TARC-4 has enhanced the formation of cellulose II by alternating their free rotation around the C5-C6 bond and the intermolecular- and intramolecular hydrogen bond networks among the polymer chains of the nanocelluloses (Altaner, Thomas, Fernandes, & Jarvis, 2014). However, cellulose II was not observed in the peaks of TAUC and ARC-4. While, MCC exhibited poor peaks of cellulose II structure along the same crystallographic plane of the nanocelluloses.

CrI is proportional to the size and rigidity of the nanocelluloses (Kim, Eom, & Wada, 2010). In this study, it is observed that ARC-4 and TARC-4 exhibited high crystalline index of 87% and 89% respectively compared to uncooled MCC (80%). This phenomenon clearly demonstrated the impact of rapid cooling on crystallinity of nanocelluloses. The further TEMPO-oxidation treatment only

slightly affect the structural properties of the rapid cool treated nanocelluloses (Kim, Eom & Wada, 2010).

3.5 Effect of rapid cooling on thermo-structural properties of the nanocelluloses

The effects of rapid cooling on the thermal stability of the nanocelluloses were investigated and compared with MCC and uncooled nanocelluloses using TGA analysis as shown in Fig. 4. The rapid weight loss observed at 270 °C for both TRC-4 and TRC-12 curves compared with TUC at $\Delta t = 28$ °C as illustrated in Fig. 4(a) can be attributed to the non-crystalline form of the nanocelluloses after rapid cooling. Moreover, the thermal degradation onset of TARC-4 and TARC-12 is 22 °C higher than that of TAUC as shown in Fig 4(b). However, ARC-4 exhibits 12 °C higher thermal degradation onset compared to ARC-12 as shown in Fig 4(c).

The thermal stability of the nanocellulose reflects their crystallinity (Peng et al., 2013; Rubentheren et al., 2016). Regardless of, the intermolecular- and intramolecular-hydrogen bonding among the nanocellulose chain structures and between the bound water and the macromolecular structure, the finite order of the macromolecular chains, and the size, and chain mobility of the nanocelluloses will affect their thermal stability (García et al., 2016; Kim et al., 2010). However, the complete pyrolysis was found at temperature range 220-375°C in all TEMPO-oxidized nanocelluloses (Fig. 5(a) and (b)).

The peak fluctuations against the chemical and rapid cooling treatments are shown by the DTG curves in Fig. 5. The complete loss of free water from the nanocelluloses was observed at 120 °C as illustrated in Fig 5. MCC exhibited higher loss of free water compared to TEMPO-oxidized CNFs, TEMPO-oxidized NCC and acid hydrolysed NCC as demonstrated in Fig. 5(a), 5b) and 5(c) respectively. The complete decomposition of the MCC was observed between 300 °C and 380 °C. While the major thermal decomposition of the acid hydrolysed NCCs was exhibited into two stages of weight loss in the DTG curves (Szcześniak, Rachocki, & Tritt-Goc, 2008), wherein ARC-4 exhibited the first stage in between 240 °C and 320 °C, and the second stage was observed at 380 °C as shown in Fig. 5(c) & (d). TAUC in Fig. 5(b) exhibited sharp peaks by overlapping first and second decomposition stage because of its strong intermolecular–hydrogen bonding among NCC chains (Novo et al., 2015; Szcześniak et al., 2008).

The peak fluctuations against the acid hydrolysis and rapid cooling treatments are shown by the DTG curves in Fig. 5(c) & (d). In AUC, the finite order of the crystallites, EOH (Fig. 2(b)) and strong intra-molecular hydrogen bonds among the cellulose chains enhanced the decomposition stability

(Åkerholm et al., 2004). Consequently, the consecutive DTG peaks of the AUC were overlapping and shifted to a high-temperature profile between 320 °C and 400 °C. While, ARC-4 exhibited prominent consecutive peaks of two-stage decomposition in the DTG curve with a degradation temperature range of 240–400 °C (reaching a leading peak at 285 °C) and the second stage at 380 °C. The peak heights and bandwidths of the ARC-4 and ARC-12 were contrary to those of AUC indicated the effects of rapid cooling on the thermal stability of ARC-4and ARC-12.

The effect of TEMPO-oxidation and rapid cooling treatment on thermo-structural properties of the nanocelluloses was illustrated in Fig 6(a) and (b) respectively. The first stage thermal decomposition of TEMPO-oxidized NCCs (TAUC and TARC-4) does not exhibited significant peak compared to TEMPO-oxidized CNFs (TUC and TRC-4) as shown in Fig. 6(a). This could be due to high crystallinity and strong intermolecular-hydrogen bonding among NCC chains of the TEMPO-oxidized NCCs compared to TEMPO-oxidized CNFs. It was also observed that the second decomposition peak was more prominent than the first decomposition stage for all the TEMPO-treated nanocelluloses based on their DTG curves as illustrated in Fig. 6(a). This phenomenon was due to the carboxylic functional moiety of the TEMPO-treated nanocelluloses.

Fig. 7(b) illustrates that both of the TRC-4 and TARC-4 exhibited lower peak height and peak area, but higher decomposition temperatures than ARC-4. TARC-4 exhibits high thermal stability of 347 °C. Thus, TRC-4 and TARC-4 show more potential intermolecular- and intramolecular-hydrogen bonding among the nanocellulose chains as well as the number of bound water molecules (Credou & Berthelot, 2014). This phenomenon demonstrates the impact of thermal heat fluctuation of the rapid cooling on TEMPO-oxidized CNFs and NCCs. Moreover, these fluctuations could be sufficient to disable the strong intermolecular hydrogen bonding among the macromolecular chains of the nanocelluloses and increased the amount of bound water during TEMPO-oxidation (Credou & Berthelot, 2014). Therefore, the bound water could strengthen the hydrogen bonds among the cellulose macro-molecules in the crystalline system via EOH (Fig. 2(b)) and enhance the thermal stability of the nanocelluloses (Fielden, Newton O'brien, Rowe, 1988, Scheirs, Camino, Tumiatti, 2001).

4 Conclusion

The effect of rapid cooling on the thermo-structural properties of the TEMPO-oxidized nanocelluloses was studied via FTIR, TGA-DTG, and XRD analyses. The study reveals that the rapid cooling treatment is a sophisticated technique that can be used to improve thermo-structural properties of the nanocelluloses. The rapid cooling treatment is a mechanical process, wherein an external thermal energy interrupts the polymeric chain network, thermal stability and intermolecular and intra-molecular hydrogen bonding of the nanocelluloses. Consequently, rapid cooling treatment remarkably affects the pseudo 2_I helical conformation of the cellulose structure. The posteriori study of the FTIR on the hydrogen bond intensity, and the hydrogen bond energy has shown that the TEMPO-oxidized nanocelluloses are significantly different from acid hydrolysed nanocellulose with respect to rapidly cooling. The crystallinity index of both of the acid hydrolyzed and the TEMPO-oxidized nanocelluloses has been improved after rapid cooling. Thermograph of the TGA-DTG analyses has shown that the stepwise thermal decomposition of the rapidly cooled and uncooled nanocelluloses was completely different for both of the TEMPO-oxidized and acid hydrolyzed nanocelluloses. In this study, the use of both TEMPO-oxidation and rapid cooling treatment on cellulose has contributed to the fabrication of NCCs with a high number of carboxyl entities and admirable thermal stability. The yield for nanocelluloses prepared from both of the acid hydrolysis and TEMPO-oxidation method had enhanced by rapid cooling treatment compared to uncooled nanocelluloses. These results show that the produced NCCs which are treated with both of the Tempo-oxidation and rapid cooling could be more effective for their uses in numerous applications, particularly as reinforcement of polymer based nanocomposite materials.

Acknowledgment: The authors would like to acknowledge the financial support from the Ministry of Education Malaysia: UM.C/625/1/HIR/MOE/ENG/52 and FP053-2015A; and University Malaya research grant: RP011A-13AET, PG159-2016A, RU022A-2014, RP024C-13AET, RU018I-2016, RU019-2015, RG031-15AET and for the success of this project.

Reference

Abitbol, T., Rivkin, A., Cao, Y., Nevo, Y., Abraham, E., Ben-Shalom, T., Lapidot, S.,Shoseyov, O. (2016). Nanocellulose, a tiny fiber with huge applications. *Current opinion in biotechnology,* 39, 76-88.

Åkerholm, M., Hinterstoisser, B., & Salmén, L. (2004). Characterization of the crystalline structure of cellulose using static and dynamic FT-IR spectroscopy. *Carbohydrate research,* 339(3), 569-578.

Altaner, C. M., Thomas, L. H., Fernandes, A. N., & Jarvis, M. C. (2014). How cellulose stretches: synergism between covalent and hydrogen bonding. *Biomacromolecules,* 15(3), 791-798.

Aulin, C., Ahola, S., Josefsson, P., Nishino, T., Hirose, Y., Österberg, M., & Wågberg, L. (2009). Nanoscale Cellulose Films with Different Crystallinities and Mesostructures-Their Surface Properties and Interaction with Water. *Langmuir,* 25(13), 7675-7685.

Baird, M. S., Hamlin, J. D., O'Sullivan, A., & Whiting, A. (2008). An insight into the mechanism of the cellulose dyeing process: Molecular modelling and simulations of cellulose and its interactions with water, urea, aromatic azo-dyes and aryl ammonium compounds. *Dyes and Pigments,* 76(2), 406-416.

Cao, X., Dong, H., & Li, C. M. (2007). New nanocomposite materials reinforced with flax cellulose nanocrystals in waterborne polyurethane. *Biomacromolecules,* 8(3), 899-904.

Carlsson, D. O., Lindh, J., Nyholm, L., Strømme, M., & Mihranyan, A. (2014). Cooxidant-free TEMPO-mediated oxidation of highly crystalline nanocellulose in water. *Rsc Advances,* 4(94), 52289-52298.

Carrillo, F., Colom, X., Sunol, J., & Saurina, J. (2004). Structural FTIR analysis and thermal characterisation of lyocell and viscose-type fibres. *European Polymer Journal,* 40(9), 2229-2234.

Chen, P., Yu, H., Liu, Y., Chen, W., Wang, X., & Ouyang, M. (2013). Concentration effects on the isolation and dynamic rheological behavior of cellulose nanofibers via ultrasonic processing. *Cellulose,* 20(1), 149-157.

Ching, Y. C., Ali, M. E., Abdullah, L. C., Choo, K. W., Kuan, Y. C., Julaihi, S. J., Chuah, C. H., Liou, N.-S. (2016). Rheological properties of cellulose nanocrystal-embedded polymer composites: a review. *Cellulose,* 23(2), 1011-1030.

Ching, Y.C., Rahman, A., Ching, K.Y., Sukiman, N.L., Cheng, H.C. (2015).Preparation and characterization of polyvinyl alcohol-based composite reinforced with nanocellulose and nanosilica. *BioResources,* 10, 3364–3377.

Choo, K.W., Ching, Y.C., Chuah, C.H., Sabariah, J., Liou, N.S. (2016). Preparation and characterization of polyvinyl alcohol-chitosan composite films reinforced with cellulose nanofiber. *Materials*, 9, 644-652.

Corgié, S. C., Smith, H. M., & Walker, L. P. (2011). Enzymatic transformations of cellulose assessed by quantitative high-throughput fourier transform infrared spectroscopy (QHT-FTIR). *Biotechnology and bioengineering,* 108(7), 1509-1520.

Credou, J., & Berthelot, T. (2014). Cellulose: from biocompatible to bioactive material. *Journal of Materials Chemistry B,* 2(30), 4767-4788.

Csoka, L., Hoeger, I. C., Peralta, P., Peszlen, I., & Rojas, O. J. (2011). Dielectrophoresis of cellulose nanocrystals and alignment in ultrathin films by electric field-assisted shear assembly. *Journal of colloid and interface science,* 363(1), 206-212.

De France, K. J., Chan, K. J., Cranston, E. D., & Hoare, T. (2016). Enhanced mechanical properties in cellulose nanocrystal–poly (oligoethylene glycol methacrylate) injectable nanocomposite hydrogels through control of physical and chemical cross-linking. *Biomacromolecules,* 17(2), 649-660.

De France, K. J., Yager, K. G., Hoare, T., & Cranston, E. D. (2016). Cooperative Ordering and Kinetics of Cellulose Nanocrystal Alignment in a Magnetic Field. *Langmuir*.

De Nooy, A. E., Besemer, A. C., & van Bekkum, H. (1995). Highly selective nitroxyl radical-mediated oxidation of primary alcohol groups in water-soluble glucans. *Carbohydrate research,* 269(1), 89-98.

Eichhorn, S. J., Dufresne, A., Aranguren, M., Marcovich, N., Capadona, J., Rowan, S., Weder, C., Thielemans, W., Roman, M., Renneckar, S., Gindl, W., Veigel, S., Keckes, J., Yano, H., Abe, K., Nogi, M., Nakagaito, A., Mangalam, A., Simonsen, J., Benight, A., Bismarck, S., Berglund, L., Peijs, T. (2010). Review: current international research into cellulose nanofibres and nanocomposites. *Journal of materials science,* 45(1), 1.

El Miri, N., El Achaby, M., Fihri, A., Larzek, M., Zahouily, M., Abdelouahdi, K., Barakat, A.,Solhy, A. (2016). Synergistic effect of cellulose nanocrystals/graphene oxide nanosheets as functional hybrid nanofiller for enhancing properties of PVA nanocomposites. *Carbohydrate polymers,* 137, 239-248.

Eyley, S., & Thielemans, W. (2014). Surface modification of cellulose nanocrystals. *Nanoscale,* 6(14), 7764-7779.

Fan, M., Dai, D., & Huang, B. (2012). Fourier transform infrared spectroscopy for natural fibres. *Fourier transform–materials analysis. InTech*.

Fielden, K., Newton, J. M., O'brien, P., & Rowe, R. C. (1988). Thermal studies on the interaction of water and microcrystalline cellulose. *Journal of pharmacy and pharmacology,* 40(10), 674-678.

Fujisawa, S., Okita, Y., Fukuzumi, H., Saito, T., & Isogai, A. (2011). Preparation and characterization of TEMPO-oxidized cellulose nanofibril films with free carboxyl groups. *Carbohydrate polymers,* 84(1), 579-583.

García, Y., Ruiz-Blanco, Y. B., Marrero-Ponce, Y., & Sotomayor-Torres, C. (2016). Orthotropic Piezoelectricity in 2D Nanocellulose. *Scientific Reports,* 6.

Goh, K.Y., Ching, Y.C., Chuah, C.H., Luqman, C.A., Liou, N.S. (2016).Individualization of microfibrillated celluloses from oil palm empty fruit bunch: Comparative studies between acid hydrolysis and ammonium persulfate oxidation. *Cellulose*, 23, 379–390.

Habibi, Y., Chanzy, H., & Vignon, M. R. (2006). TEMPO-mediated surface oxidation of cellulose whiskers. *Cellulose,* 13(6), 679-687.

Hamad, W. Y., & Hu, T. Q. (2010). Structure–process–yield interrelations in nanocrystalline cellulose extraction. *The Canadian Journal of Chemical Engineering,* 88(3), 392-402.

Helbert, W., Cavaille, J., & Dufresne, A. (1996). Thermoplastic nanocomposites filled with wheat straw cellulose whiskers. Part I: processing and mechanical behavior. *Polymer composites,* 17(4), 604-611.

Henriksson, M., & Berglund, L. A. (2007). Structure and properties of cellulose nanocomposite films containing melamine formaldehyde. *Journal of Applied Polymer Science,* 106(4), 2817-2824.

Hermans, P., & Weidinger, A. (1948). Quantitative X-Ray Investigations on the Crystallinity of Cellulose Fibers. A Background Analysis. *Journal of Applied Physics,* 19(5), 491-506.

Isogai, T., Saito, T., & Isogai, A. (2011). Wood cellulose nanofibrils prepared by TEMPO electro-mediated oxidation. *Cellulose,* 18(2), 421-431.

Jonoobi, M., Oladi, R., Davoudpour, Y., Oksman, K., Dufresne, A., Hamzeh, Y., & Davoodi, R. (2015). Different preparation methods and properties of nanostructured cellulose from various natural resources and residues: a review. *Cellulose,* 22(2), 935-969.

Kalita, E., Nath, B., Deb, P., Agan, F., Islam, M. R., & Saikia, K. (2015). High quality fluorescent cellulose nanofibers from endemic rice husk: Isolation and characterization. *Carbohydrate polymers,* 122, 308-313.

Khalil, H. A., Davoudpour, Y., Islam, M. N., Mustapha, A., Sudesh, K., Dungani, R., & Jawaid, M. (2014). Production and modification of nanofibrillated cellulose using various mechanical processes: a review. *Carbohydrate polymers,* 99, 649-665.

Kim, U.-J., Eom, S. H., & Wada, M. (2010). Thermal decomposition of native cellulose: influence on crystallite size. *Polymer Degradation and Stability,* 95(5), 778-781.

Lee, C. M., Kubicki, J. D., Fan, B., Zhong, L., Jarvis, M. C., & Kim, S. H. (2015). Hydrogen-Bonding Network and OH Stretch Vibration of Cellulose: Comparison of Computational Modeling with Polarized IR and SFG Spectra. *The Journal of Physical Chemistry B,* 119(49), 15138-15149.

Li, B., Cao, J., Cao, X., Guo, B., & Lu, H. (2016). Preparation and Characterization of Chemically Crosslinked Polyvinyl Alcohol/Carboxylated Nanocrystalline Cellulose Nanocomposite Hydrogel Films with High Mechanical Strength. *Journal of Macromolecular Science, Part B,* 55(5), 518-531.

Li, J., Wei, X., Wang, Q., Chen, J., Chang, G., Kong, L., Su. J., Liu, Y. (2012). Homogeneous isolation of nanocellulose from sugarcane bagasse by high pressure homogenization. *Carbohydrate polymers,* 90(4), 1609-1613.

Lu, A., Hemraz, U., Khalili, Z., & Boluk, Y. (2014). Unique viscoelastic behaviors of colloidal nanocrystalline cellulose aqueous suspensions. *Cellulose,* 21(3), 1239-1250.

Martinez-Felipe, A., Cook, A. G., Abberley, J. P., Walker, R., Storey, J. M., & Imrie, C. T. (2016). An FT-IR spectroscopic study of the role of hydrogen bonding in the formation of liquid crystallinity for mixtures containing bipyridines and 4-pentoxybenzoic acid. *Rsc Advances,* 6(110), 108164-108179.

Mhd Haniffa, M. A. C., Ching, Y. C., Abdullah, L. C., Poh, S. C., & Chuah, C. H. (2016). Review of bionanocomposite coating films and their applications. *Polymers,* 8(7), 246.

Missoum, K., Belgacem, M. N., & Bras, J. (2013). Nanofibrillated cellulose surface modification: a review. *Materials,* 6(5), 1745-1766.

Mok, C.F., Ching, Y.C., Muhamad, F., Abu Osman, A. & Ramesh, S. (2017). Poly(vinyl alcohol)-α-chitin composites reinforced by oil palm empty fruit bunch fiber-derived nanocellulose. *Inter. J. Polymer Analysis and Characterization,* http://dx.doi.org/10.1080/1023666X.2017.1288345.

Montanari, S., Roumani, M., Heux, L., & Vignon, M. R. (2005). Topochemistry of carboxylated cellulose nanocrystals resulting from TEMPO-mediated oxidation. *Macromolecules,* 38(5), 1665-1671.

Morán, J. I., Alvarez, V. A., Cyras, V. P., & Vázquez, A. (2008). Extraction of cellulose and preparation of nanocellulose from sisal fibers. *Cellulose,* 15(1), 149-159.

Munier, P., Gordeyeva, K., Bergström, L., & Fall, A. B. (2016). Directional freezing of nanocellulose dispersions aligns the rod-like particles and produces low-density and robust particle networks. *Biomacromolecules,* 17(5), 1875-1881.

Nandgaonkar, A., Krause, W., & Lucia, L. (2016). Fabrication of cellulosic composite scaffolds for cartilage tissue engineering. *Nanocomposites for Musculoskeletal Tissue Regeneration*, 187.

Neyertz, S., Pizzi, A., Merlin, A., Maigret, B., Brown, D., & Deglise, X. (2000). A new all-atom force field for crystalline cellulose I. *Journal of Applied Polymer Science,* 78(11), 1939-1946.

Novo, L. P., Bras, J., García, A., Belgacem, N., & Curvelo, A. A. (2015). Subcritical water: a method for green production of cellulose nanocrystals. *ACS Sustainable Chemistry & Engineering,* 3(11), 2839-2846.

Okita, Y., Fujisawa, S., Saito, T., & Isogai, A. (2010). TEMPO-oxidized cellulose nanofibrils dispersed in organic solvents. *Biomacromolecules,* 12(2), 518-522.

Pääkkö, M., Ankerfors, M., Kosonen, H., Nykänen, A., Ahola, S., Österberg, M., Ruokolainen, J., Laine, J., Ikkala, O. (2007). Enzymatic hydrolysis combined with mechanical shearing and high-pressure homogenization for nanoscale cellulose fibrils and strong gels. *Biomacromolecules,* 8(6), 1934-1941.

Peng, Y., Gardner, D. J., Han, Y., Kiziltas, A., Cai, Z., & Tshabalala, M. A. (2013). Influence of drying method on the material properties of nanocellulose I: thermostability and crystallinity. *Cellulose,* 20(5), 2379-2392.

Poletto, M., Ornaghi, H. L., & Zattera, A. J. (2014). Native cellulose: structure, characterization and thermal properties. *Materials,* 7(9), 6105-6119.

Qiu, X and Hu, S. (2013). "Smart" materials based on cellulose: A review of the preparations, properties, and applications. *Materials,* 6, 738-781.

Rubentheren, V., Ward, T.A., Chee, C.Y., Nair, P. (2015). Physical and chemical reinforcement of chitosan film using nanocrystalline cellulose and tannic acid. *Cellulose,* 22, 2529–2541.

Rubentheren, V., Thomas, A.W., Ching, Y.C., Praveena, N., Erfan, S., Christopher, F. (2016). Effects of heat treatment on chitosan nanocomposite film reinforced with nanocrystalline cellulose and tannic acid. *Carbohydr. Polym*. 140, 202–208.

Saito, T., & Isogai, A. (2004). TEMPO-mediated oxidation of native cellulose. The effect of oxidation conditions on chemical and crystal structures of the water-insoluble fractions. *Biomacromolecules,* 5(5), 1983-1989.

Saito, T., Okita, Y., Nge, T., Sugiyama, J., & Isogai, A. (2006). TEMPO-mediated oxidation of native cellulose: Microscopic analysis of fibrous fractions in the oxidized products. *Carbohydrate polymers,* 65(4), 435-440.

Salajková, M., Berglund, L. A., & Zhou, Q. (2012). Hydrophobic cellulose nanocrystals modified with quaternary ammonium salts. *Journal of Materials Chemistry,* 22(37), 19798-19805.

Salas, C., Nypelö, T., Rodriguez-Abreu, C., Carrillo, C., & Rojas, O. J. (2014). Nanocellulose properties and applications in colloids and interfaces. *Current Opinion in Colloid & Interface Science,* 19(5), 383-396.

Sampath, U.G., Ching, Y.C., Chuah, C.H., Sabariah, J.J., Lin, P.C. (2016). Fabrication of porous materials from natural/synthetic biopolymers and their composites. *Materials*, 9, 991–996.

Scheirs, J., Camino, G., & Tumiatti, W. (2001). Overview of water evolution during the thermal degradation of cellulose. *European Polymer Journal,* 37(5), 933-942.

Shafeiei-Sabet, S., Hamad, W. Y., & Hatzikiriakos, S. G. (2013). Influence of degree of sulfation on the rheology of cellulose nanocrystal suspensions. *Rheologica Acta,* 52(8-9), 741-751.

Siqueira, G., Bras, J., & Dufresne, A. (2008). Cellulose whiskers versus microfibrils: influence of the nature of the nanoparticle and its surface functionalization on the thermal and mechanical properties of nanocomposites. *Biomacromolecules,* 10(2), 425-432.

Soni, B., & Mahmoud, B. (2015). Chemical isolation and characterization of different cellulose nanofibers from cotton stalks. *Carbohydrate polymers,* 134, 581-589.

Szcześniak, L., Rachocki, A., & Tritt-Goc, J. (2008). Glass transition temperature and thermal decomposition of cellulose powder. *Cellulose,* 15(3), 445-451.

Tang, Y., Yang, S., Zhang, N., & Zhang, J. (2014). Preparation and characterization of nanocrystalline cellulose via low-intensity ultrasonic-assisted sulfuric acid hydrolysis. *Cellulose,* 21(1), 335-346.

Thennakoon, M. S. U. G. , Ching, Y. C., Chuah, C.H. (2017). Enhancement of curcumin bioavailability using nanocellulose reinforced chitosan hydrogel. *Polymers*, 9(64), doi:10.3390/polym9020064.

Thennakoon, M. S. U. G. , Ching, Y. C., Chuah, C.H., Ramesh, S., Lin, P.C. (2017). Preparation and characterization of nanocellulose reinforced semi-interpenetrating polymer network of chitosan hydrogel. *Cellulose*, 24, 2215–2228.

Thennakoon, M. S. U. G , Ching, Y.C., Kuan, Y. C. , Chuah, C. H. and Luqman, C. A. (2017). Biomedical and Microbiological Applications of Bio-Based Porous Materials: A Review. *Polymers,* 7, 9, 160; doi:10.3390/polym9050160.

Wada, M., Heux, L., & Sugiyama, J. (2004). Polymorphism of cellulose I family: reinvestigation of cellulose IVI. *Biomacromolecules,* 5(4), 1385-1391.

Yokoi, H., Nakase, T., Goto, K., Ishida, Y., Ohtani, H., Tsuge, S., Sonoda, T., Ona, T. (2003). Rapid characterization of wood extractives in wood by thermal desorption-gas chromatography in the presence of tetramethylammonium acetate. *Journal of analytical and applied pyrolysis,* 67(1), 191-200.

Zhong, L., Fu, S., Peng, X., Zhan, H., & Sun, R. (2012). Colloidal stability of negatively charged cellulose nanocrystalline in aqueous systems. *Carbohydrate polymers,* 90(1), 644-649.

Fig. 1. Comparison of FTIR spectra of MCC, TEMPO-oxidized rapid cooled NCCs (TARC-4, TARC-12), TEMPO-oxidized uncooled NCC (TAUC), acid-hydrolysed rapid cooled NCCs (ARC-4, ARC-12), acid-hydrolysed uncooled NCC (AUC), and TEMPO-oxidized rapid cooled CNFs (TRC-4, TRC-12), & TEMPO-oxidized uncooled CNF (TUC).

Fig. 2. A posteriori study on the effect of rapid cooling on peak parameters of the FTIR spectra of the nanocelluloses compared with MCC: (a) peak height ratio was used to analyze LOI, TCI, and HBI and: (b) peak area was used to analyze CS, finite order, and EOH of the nanocelluloses (TUC, TRC-4, AUC, ARC-4, TAUC, & TARC-4). CS = crystalline structure.

Fig. 3. The effect of rapid cooling on (a) X-ray diffraction pattern of MCC, acid-hydrolyzed NCCs (AUC and ARC-4) and TEMPO–oxidized NCCs (TAUC and TARC-4); (b) formation of cellulose II along the crystallographic plane of d($1\bar{1}0$) at 12.04°; (c) formation of cellulose II along the crystallographic plane of d(110) at 20.0°.

Fig. 4. Comparison TGA curves of MCC with nanocellulose (a) TEMPO-oxidized CNFs; (b) TEMPO-oxidized NCC; (c) Acid hydrolyzed NCC.

Fig. 5. Comparison of the effect of cooling treatment on complete loss of free water of MCC with (a) TEMPO-oxidized CNF; (b) TEMPO-oxidized NCC; (c) & (d) acid hydrolyzed NCC (note for (d) : 1- first stage thermal decomposition; 2- second stage thermal decomposition).

Fig. 6. The effect of rapid cooling on (a) first and second stage of thermal decompositions of the DTG curves of TEMPO-oxidized CNFs & NCCs compared to MCC. (b) DTG peak pattern with respect to the stepwise thermal decomposition of acid-hydrolysed NCC, TEMPO–oxidized CNF & NCC compared to MCC.

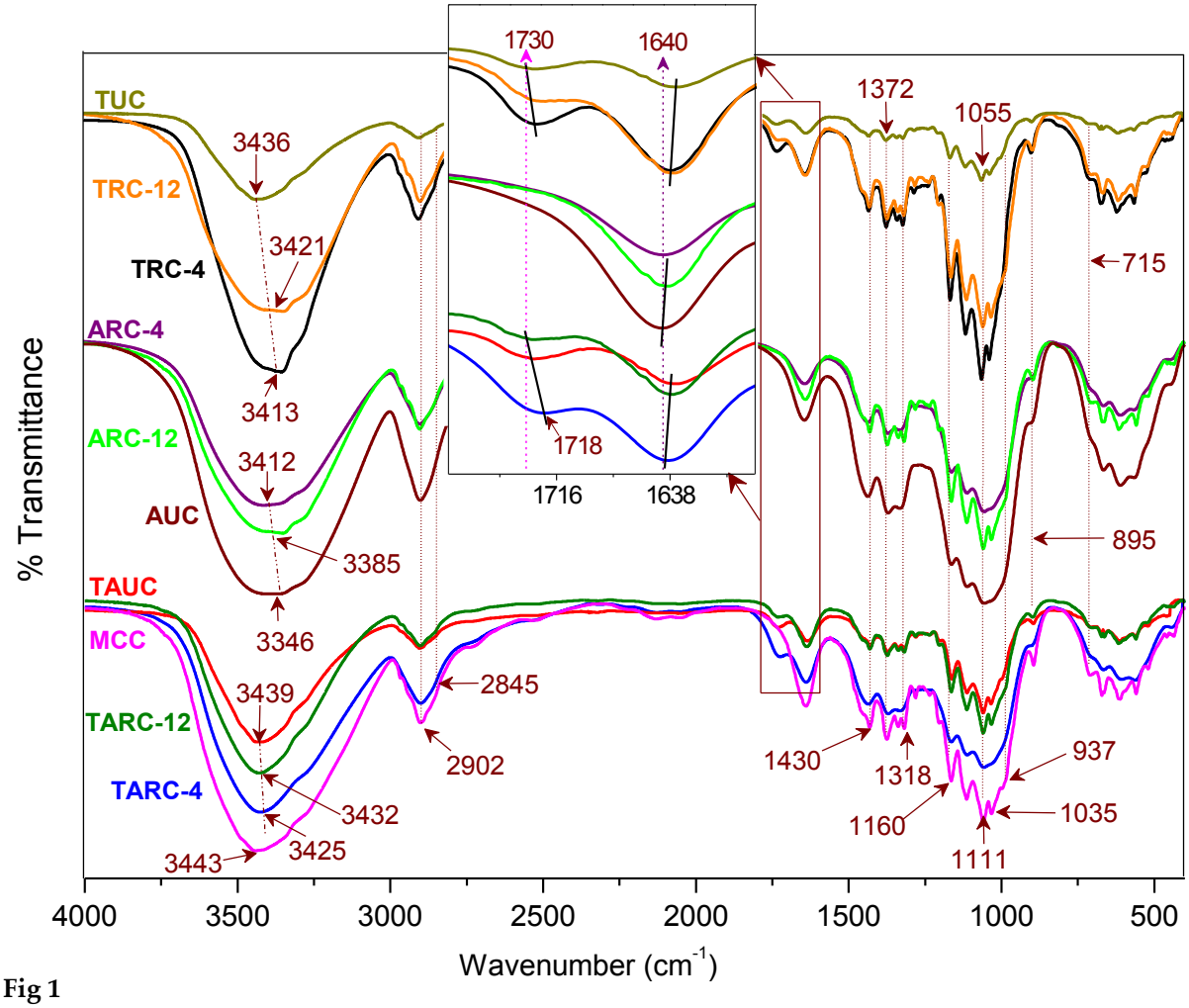

Fig 1

Fig 2

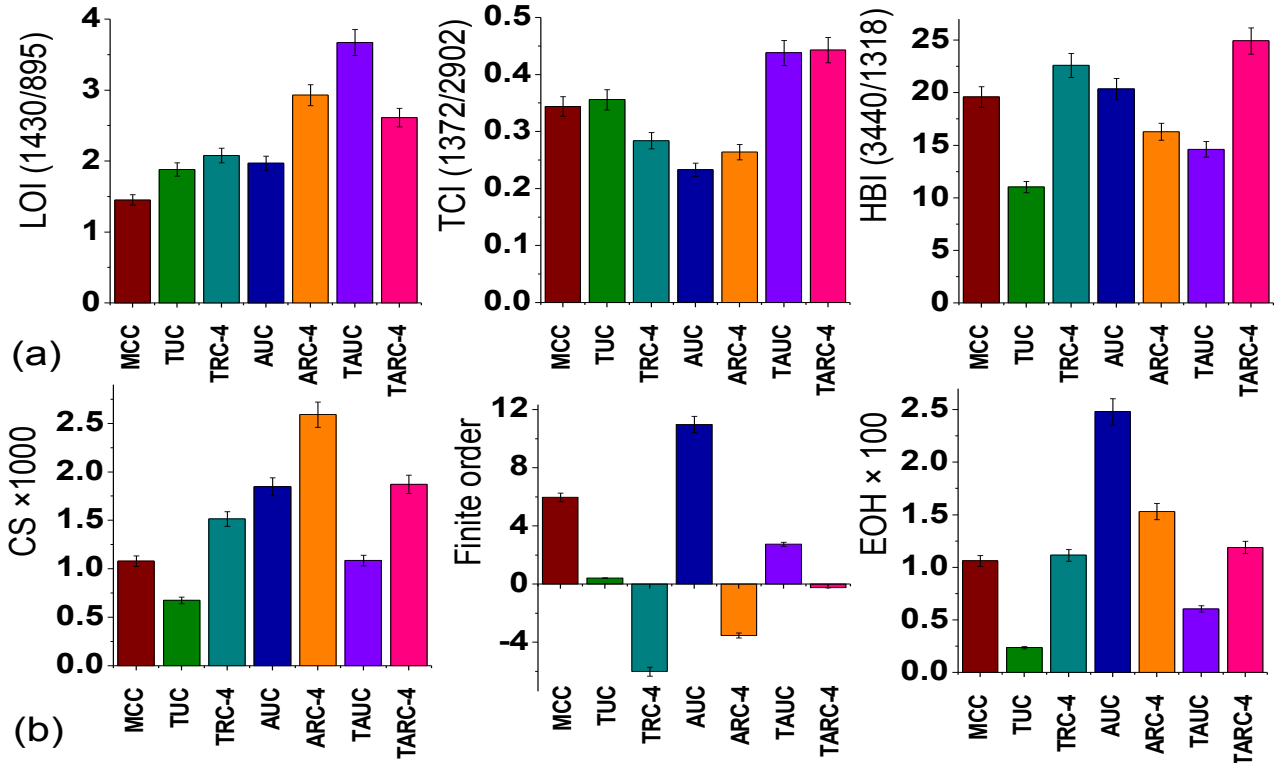

Fig 3

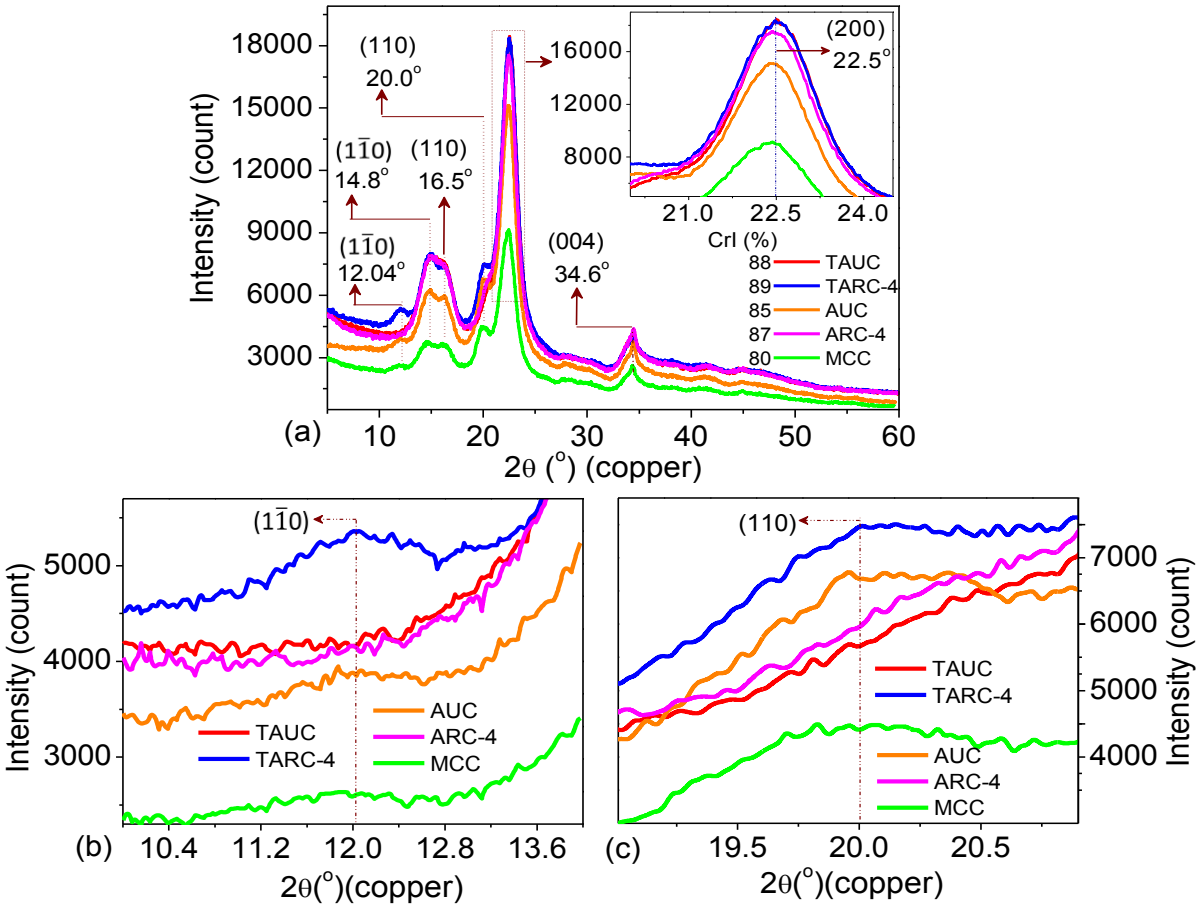

Fig 4

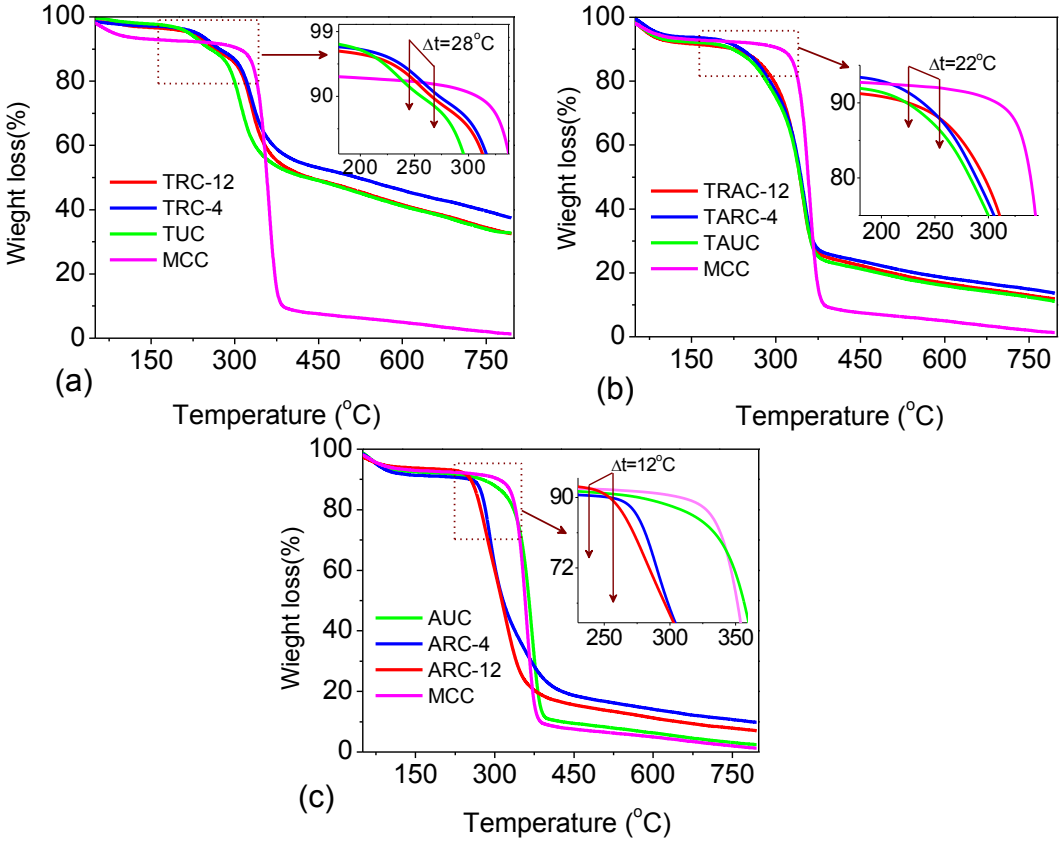

Fig 5

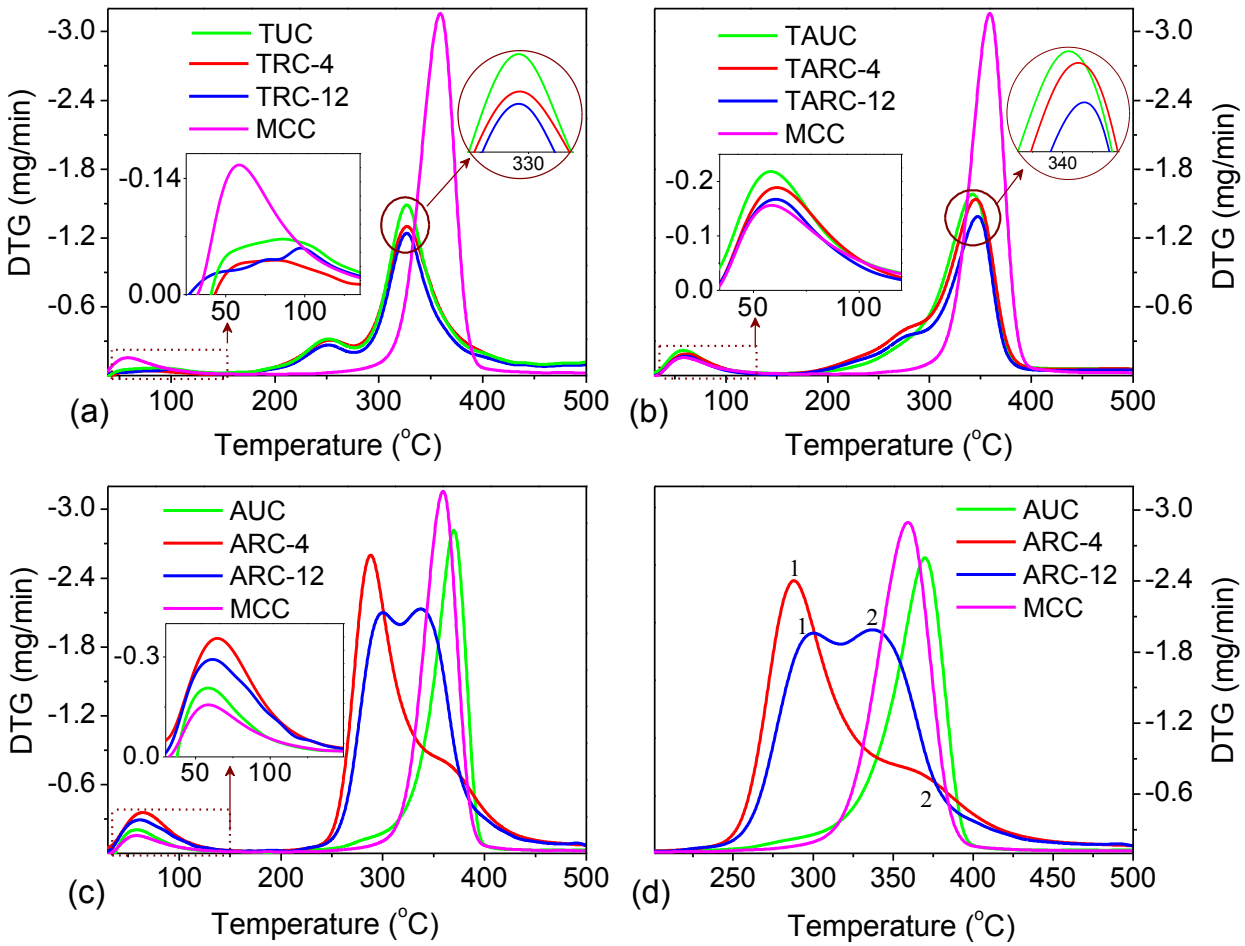

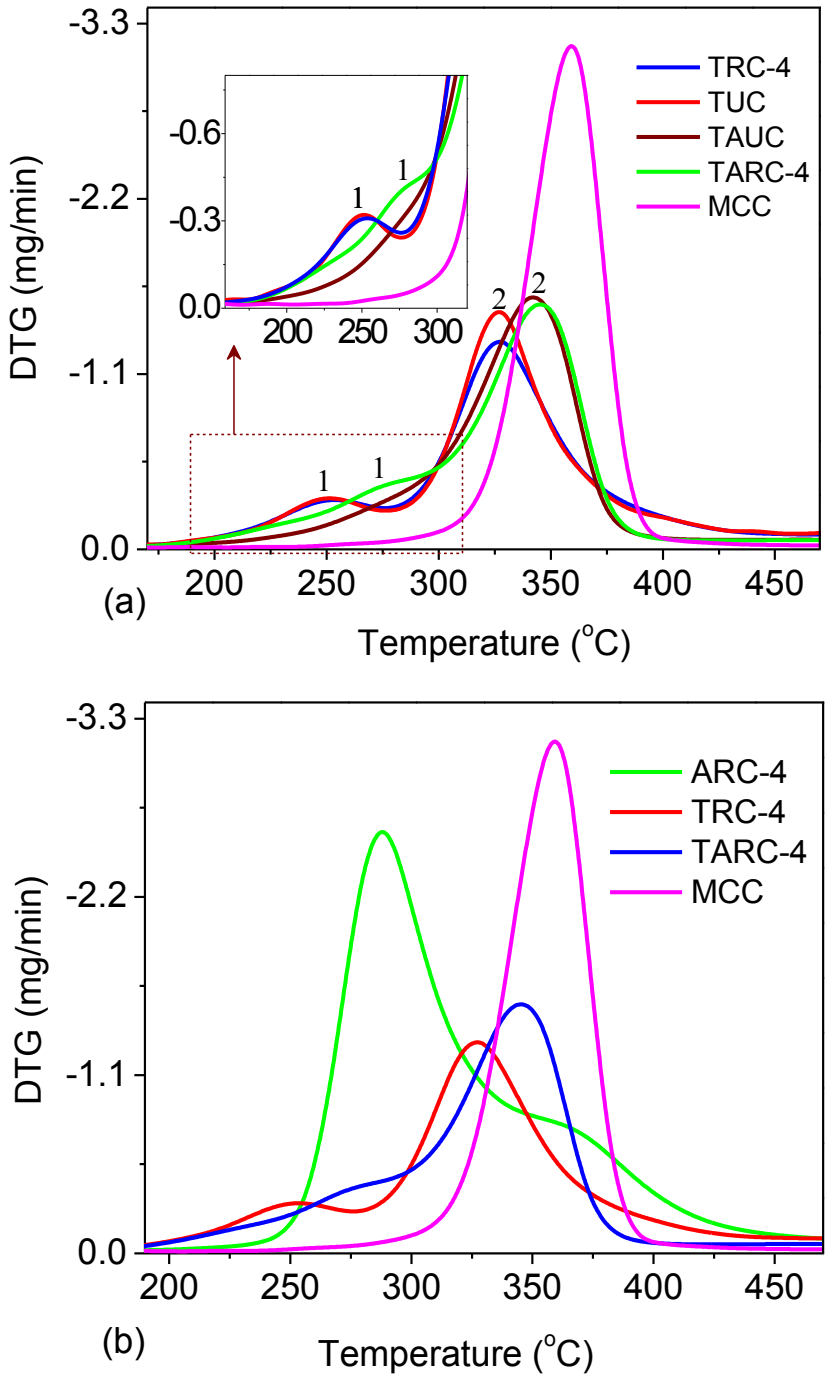

Fig 6

Table 1 The effect of rapid cooling on hydrogen bond energy and hydrogen bond distance.

Parameters	MCC	Nanocelluloses								
		TEMPO-treatment			Acid treatment			Acid &TEMPO treatment		
		TUC	TRC-12	TRC-4	AUC	ARC-12	ARC-4	TAUC	TARC-12	TARC-4
Observed frequency/ cm	3443	3436	3421	3413	3346	5	3412	3439	3432	3425
E_H value (kJ)	14.885	15.388	16.542	17.042	21.860	)59	17.114	15.172	15.682	16.179
R value (Å)	2.805	2.803	2.788	2.799	2.783	31	2.798	2.803	2.794	2.800
Yield (%)	-	15.68	23.27	48.08	90.82	19	91.71	62.98	68.73	72.54